Desalination and Water Treatment
www.deswater.com

doi: 10.5004/dwt.2018.21992

105 (2018) 310–321
February

Photocatalytic oxidation of methyl orange in water using Fe-Zn co-doped TiO_2 under different wavelengths

Rongfang Yuan, Shaona Wang, Dan Liu, Beihai Zhou*

Beijing Key Laboratory of Resource-oriented Treatment of Industrial Pollutants, Department of Environmental Engineering, University of Science and Technology Beijing, Beijing 100083, China, email: yuanrongfang@ustb.edu.cn (R. Yuan), wangsn1991@163.com (S. Wang), ustbldan@126.com (D. Liu), zhoubeihai@sina.com (B. Zhou)

Received 4 October 2017; Accepted 1 February 2018

ABSTRACT

Photocatalytic oxidation could be used to effectively decompose methyl orange (MO) in water. The 500°C calcined 0.0010% Fe-Zn co-doped TiO_2 with the Fe:Zn radio of 3:2 showed highest photocatalytic activity, corresponding to the MO removal efficiency of 75.5% and pseudo-first-order rate constant of 0.280/h. The effectiveness order of xenon lamp was 365 nm > 254 nm > 420 nm > 475 nm. MO degradation under 365 nm irradiation was faster because of the better penetrability of light at 365 nm than at 254 nm. The structures of the intermediates formed during photocatalytic oxidation process were mainly based on demethylation, benzene ring opening and azo bond cleaving. Almost all the pollutant was decomposed to be the inorganic substance. The elimination of MO in photocatalytic oxidation process by granular activated carbon (GAC) supported Fe-Zn co-doped TiO_2 was higher than by dispersive co-doped TiO_2. GAC coated with 15-layer TiO_2 was proved to be the best composition with respect to photocatalytic activity, with the MO removal efficiency of 92.5%. This number was still over 80% after using for 3 times, indicating that cyclic usage of the photocatalysts is possible. Moreover, the photocatalytic activity of the catalysts could be improved from 84.3% to 89.7% by drying.

Keywords: Fe-Zn co-doped TiO_2; Photocatalytic oxidation; Wavelength; Methyl orange; Mechanism

1. Introduction

Wastewater from the textile industry contains large amounts of organic dyes, representing a major threat to the environment due to their toxicity and potentially carcinogenic nature. Among the dyes, azo dyes constitute the largest group of dyes and represent more than half of the global dye production [1]. The classical methods are often ineffective to mineralize these pollutants in wastewater. Heterogeneous photocatalysis has proved its effectiveness and adopted as an alternative technique compared to the classical ones because of its ability to eliminate totally the organic substances without any toxic transformation or transfer to another environment and also it is mostly non-selective [2].

Among various semiconductors, TiO_2 has been considered as the most promising catalyst for eliminating environmental contaminants in water. However, it suffers from wide band gap energy (E_g) and high recombination rate of charge carriers [3]. To address these problems, ions have been doped into TiO_2 to increase the photocatalytic activity [4,5] as well as enhance the wavelength of light which can excite TiO_2 catalysts [6,7].

Simultaneously doping of two or three dopants into TiO_2 could significantly enhance its photocatalytic activity as compared to the enhancement through single element doping [8,9]. Naraginti found the synergetic effects of Ag-Sr co-doping in TiO_2 made the catalysts to trap electrons and holes, leading to higher photocatalytic activity compared to Ag-doped TiO_2 [10]; Eskandarloo reported that the Sm-Ce co-doped TiO_2 catalyst with narrower E_g showed higher activity compared with mono-doped TiO_2 [11]; Hou indicated the novel Fe-Er co-doped TiO_2 showed a superbly enhanced photocatalytic activities compared to the Er-TiO_2

*Corresponding author.

and Fe-TiO_2 [8]. However, the rare-earth metals, which were used in the above mentioned studies, have potential hazardous effect on human bodies. As the introduction of Fe^{3+} or Zn^{2+} into TiO_2 matrix leads to the enhancement of the photocatalytic activity [12], the metals of Fe and Zn are suitable to be used for doping [13].

The wavelength of the light source can affect the photocatalytic efficiency of the pollutants in the presence of TiO_2 catalysts with different E_g. Researches indicated the degradation of the pollutants was the fastest under 254 nm irradiation, and depended on the light source energy (254 nm > 310 nm > 365 nm > solar light) [14,15], but Gupta found highest removal efficiency was obtained under 365 nm irradiation [16]. However, less is known about the photocatalytic efficiency at longer wavelength.

In addition, there are some drawbacks in using TiO_2 in powder form, such as the difficulty in separating TiO_2 from water, and the aggregation of TiO_2 especially calcined at high concentrations [17]. This deficiency can be avoided by coating TiO_2 on substrates [18].

Nowadays, methyl orange (MO) solution has often been selected as the model compound to simulate the industrial wastewater [19]. In this study, photocatalytic properties of the photocatalysts for the decomposition of MO under different wavelengths of the light source were estimated. Based on the experimental observations, a degradation pathway of MO over photocatalytic oxidation has also been proposed. Moreover, the photocatalytic activity and repeatability of the substrates supported TiO_2 for the degradation of MO were investigated.

2. Materials and methods

2.1. Material

Tetrabutyl orthotitanate ($C_{16}H_{36}O_4Ti$) (analytical reagent) was purchased from Tianjin Kemiou Chemical Reagent Co., Ltd. MO (chemical purity) was purchased from Tianjin Guangfu Fine Chemical Research Institute. $FeCl_3{\cdot}6H_2O$ and $ZnCl_2$ with analytical reagent grade were purchased from Beijing Chemical Reagent Company. Granular active carbon (GAC), with the particle size of 2–3 mm, was purchased from Tianjin Fuchen chemical reagent company.

The photocatalytic reactor was a cylindrical glass column with diameter and height of 100 and 200 mm, respectively; a xenon lamp (HSX-F300, Beijing NBET Technology Co., Ltd) with the electric current of 15 A was found above the reactor (Fig. 1). Color absorbers with transmitted light of 254 ± 15, 365 ± 15, 420 ± 15 and 475 ± 15 nm, which was made of High permeable quartz, were used to filter the light. O_2 gas was prepared by an oxygenerator (Beijing North Star Yaao Scitech Co., Ltd, China), and the gas was fed into the reactor through a 4–7 μm porous glass core aeration plate.

2.2. Preparation and characterization of TiO_2

Tetrabutyl orthotitanate of 0.2 mol was dissolved in 120 mL ethyl alcohol, and the obtained mixed solution was stirred for 2 h. Afterward, $FeCl_3$ or $ZnCl_2$ (0–10 μmol), glacial acetic acid (80 mL), ethyl alcohol (120 mL) and Milli-Q water (30 mL) were mixed together and added into the mixed solution in drops. The final mixed solution was standing at 30°C for 7 d to form wet gel. Then the wet gel was dried at 105°C

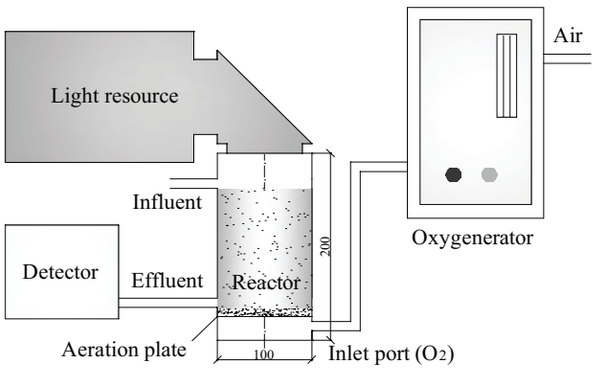

Fig. 1. Laboratory-scale photocatalytic oxidation contactor.

to form dry gel powder. Lastly, the dry gel powder was heated at 450, 500 or 550°C for 5 h, and the nanometer-sized TiO_2, with the Fe- or Zn-doping amount of 0%–0.0050% (atomic percentage), was obtained after adequate mulling. Scanning electron microscopic (SEM) images were obtained with a ZEISS ULTRA 55 Field-Emission Scanning Electron Microscope (Carl Zeiss, Germany). X-ray diffraction (XRD) patterns of TiO_2 were collected in a Rigaku Dmax-RB diffractometer (Tokyo, Japan). The BET surface areas (S_{BET}) were determined using a Quadrasorb SI-MP apparatus (Quantachrome Instrument, USA). Diffuse reflectance spectroscopy (DRS) was performed with a HITACHI U-3010 UV-Vis scanning spectrophotometer (Tokyo, Japan).

GAC was soaked in 5% HCl solution for 12 h to remove any impurity, washed with distilled water repeatedly to pH 7, and dried overnight at 105°C. The substrates were immersed in the wet gel for 15 min, lifted by dip coater at a speed of 900 μm/s, and then dried at 105°C. Different GAC supported TiO_2 catalytic systems with different TiO_2 amount were prepared by immersing and drying the as-prepared catalysts repeatedly, followed by calcining them at 500°C for 5 h. GAC was coated for 1, 5, 10, 15 and 20 layers, equivalent to the TiO_2 mass percentage of about 0.1%, 0.5%, 1%, 3% and 5%, respectively.

2.3. Photocatalytic activity tests

All oxidation experiments were carried out at 20°C and initial pH 7.0. The aqueous slurry of 1000 mL, with 15 mg/L MO and 0.5 g/L TiO_2, was stirred and bubbled with O_2 (80–100 mL/min) for 30 min prior to irradiation, and stirred by a magnetic stirring apparatus at 100 r/min. The sample was taken out of the reactor at 30 min intervals, and clear solution was obtained after centrifugation at 2000 r/min. The MO concentrations were determined using a UV-Vis spectrophotometer (Hach DR5000, USA) at a wavelength of 462 nm.

The MO removal efficiencies in the presence of GAC supported TiO_2 were detected by the same method with that of the above mentioned experiment, except that 20 cm^3 of the catalyst was invited instead of 0.5 g of the unsupported ones, corresponding to the TiO_2 amount of 0.01, 0.05, 0.1, 0.3 and 0.5 g for the 1, 5, 10, 15 and 20 layers coating catalysts, respectively. The tests were repeated for several times to investigate the repeatability of the catalyst. In order to obtain the oxidation products of MO

under 365 nm UV irradiation with and without the Fe-Zn co-doped catalyst, 200 mL MO solution, with MO initial concentration of 15 mg/L, was used. Oxidation products of MO were analyzed using liquid chromatography tandem mass spectrometry (LC-MS/MS) (Agilent 1290LC coupled with 6460 MS/MS) equipped with an Agilent Zorbax SB-C18 (2.1 mm × 100 mm, 1.8 μm) HPLC column. The mobile phase was composed of acetonitrile and 0.1% formic acid in ultrapure water, and the flow rate was 0.3 mL/min. The sample injection volume was 10 μL. The MS detection modes for product identification were MS2 scan and MS2 product ion scan.

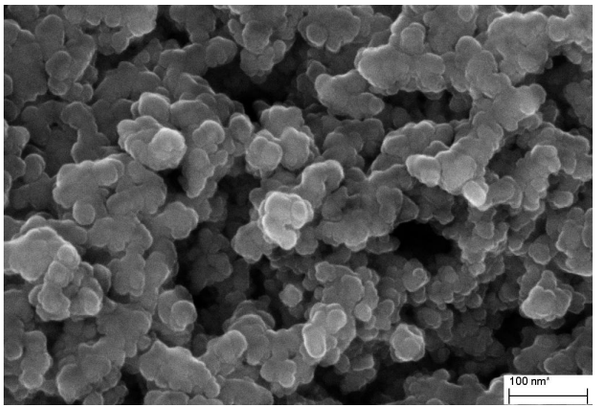

Fig. 2 .SEM image of 0.0010% Fe-Zn (3:2) co-doped TiO_2 calcined at 500°C.

3. Results and discussion

3.1. Photocatalyst characterization of the TiO_2 nanoparticles

3.1.1. SEM analysis

The SEM morphology of 0.0010% Fe-Zn (3:2) co-doped TiO_2 calcined at 500°C indicates that the TiO_2 nanoparticles are globular and agglomerated. The diameter of the co-doped TiO_2 was in the range of 10-30 nm.

3.1.2. XRD analysis

It can be seen from the XRD patterns of TiO_2 (Fig. 3) that the crystallite phase containing Fe and Zn metal oxides was not observed in the XRD patterns. For Fe-doped TiO_2, the ionic radii of Fe^{3+} (55 pm) was smaller than that of Ti^{4+} (60.5 pm), and Fe^{3+} could highly disperse in TiO_2 lattice [2].

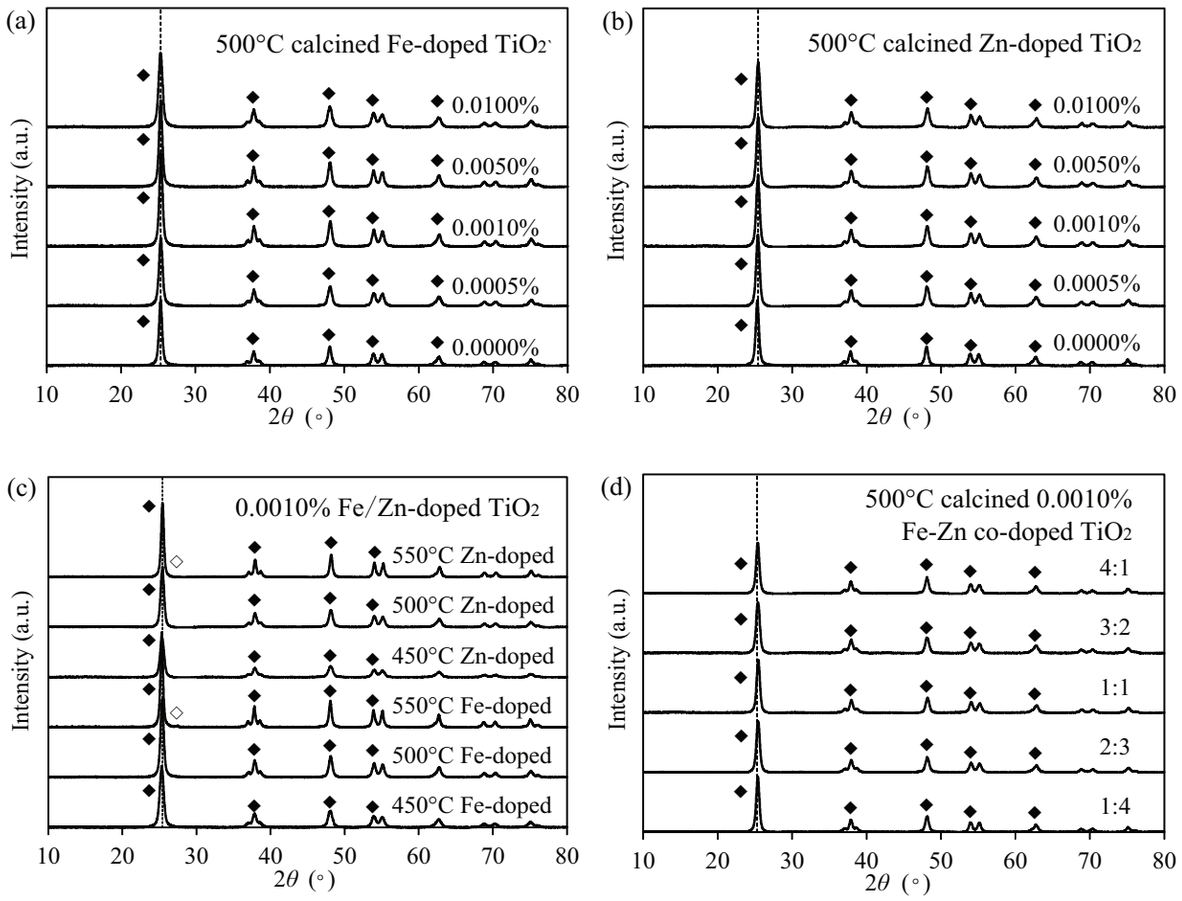

Fig. 3. XRD patterns of TiO_2. "◆" refers to the anatase phase, and "◇" refers to the rutile phase.

For Zn-doped TiO_2, Zn^{2+} ions were dispersed in the bulk of TiO_2 partially, while ZnO was also formed on the surface of TiO_2 because of the larger ionic radii of Zn^{2+} ions (74 pm). The peak of ZnO was not observed because their metal sites were below the visibility limit of X-ray analysis [20].

The diffraction peaks belonging to anatase phase (2θ of about 25.3°) in Fe- or Zn-doped TiO_2 decreased with increasing doping amount because the substitution of the doping ions lowered the crystallization of TiO_2 [21]. When the calcination temperature raised from 450°C to 550°C, the diffraction peak of anatase appeared stronger and sharper, indicating better crystallites were formed; for the 550°C calcined catalyst, the (110) crystal plane of rutile phase (located at about 27.4°) appeared due to the transformation from anatase phase to rutile phase.

For the 0.0010% Fe-Zn co-doped TiO_2 calcined at 500°C, the 2θ positions and peak intensities did not change significantly when the Fe:Zn ratio changed. Only anatase phase was found in the catalysts.

The average crystallite sizes for all samples (Table 1) were calculated from the full width at half maximum of the (101) anatase peak according to the Scherrer's formula, and they were in the range of 10–30 nm. Differences of the crystallites sizes among the catalysts with diffident dopant amount were not obvious. However, rising of the calcination temperature caused the increase of the crystallites sizes for the catalysts.

3.1.3. Surface analysis

It has been reported that larger S_{BET} indicated more pollutants were adsorbed onto the surface of catalyst where the pollutants could be decomposed, and more areas were supplied for electron-hole separation. Table 1 shows that the S_{BET} of the TiO_2 decreased as the calcination temperature increase because of the aggregation of the nanoparticles. In addition, for the catalysts calcined at 450 and 500°C, the S_{BET} increased with an increase in the Fe^{3+} or Zn^{2+} amount doped in TiO_2 catalyst, attributing to the segregation of the dopant cations at the grain boundary, which inhibited grain growth by restricting the coalescence of some smaller neighboring grains [22]. However, for the catalysts calcined at 550°C, when the doping amount of Fe^{3+} or Zn^{2+} increased, the S_{BET} increased at first, and then decreased. The reduction in the S_{BET} may be caused by the blocking of fine capillaries of parent TiO_2 surface by metal film islands [20].

The S_{BET} for the 0.0010% Fe-Zn co-doped TiO_2 calcined at 500°C, with the Fe:Zn ratio of 1:4, 2:3, 1:1, 3:2 and 4:1 were 95, 103, 106, 115 and 101 m^2/g, respectively, larger than those of the Fe- or Zn-doped TiO_2. Doping of a second metal changed the catalyst surface structure because of the conservation of a large number of micropores [3].

3.1.4. UV-Vis DRS analysis

The UV-Vis DRS analysis was conducted to obtain the *Eg* of the undoped, Fe-doped, Zn-doped or Fe-Zn co-doped TiO_2 (Fig. 4 and Tables 1). TiO_2 calcined at higher temperatures showed a tendency to red shift, which resulted from the narrower *Eg* of rutile TiO_2 compared with that of anatase TiO_2. The *Eg* of undoped TiO_2 ranged from 2.92 to 3.11 eV, while those for Fe-doped TiO_2 and Zn-doped TiO_2 were 2.80–3.08 eV and 2.90–3.10 eV, respectively. The introduction of the dopants into TiO_2 matrix led to enhancement in absorption of light, extending the spectral response of the photocatalysts [23]. In addition, by increasing the content of Fe^{3+} or Zn^{2+}, the absorptions of the catalysts were significantly enhanced, and the E_g were hence decreased [20].

The *Eg* of the 0.0010% Fe-Zn co-doped TiO_2 calcined at 500°C, with the Fe:Zn ratio of 1:4, 2:3, 1:1, 3:2 and 4:1 were 2.95, 2.93, 2.92, 2.91 and 2.91 eV, respectively, between those of the Fe-doped and Zn-doped TiO_2.

3.2. Photocatalytic activity of the TiO_2 nanoparticles

3.2.1. Photocatalytic oxidation of MO

Fig. 5(a)–(d) show the influence of the calcination temperature and the dopants in the catalyst on the degradation of MO under irradiation with the wavelength of 365 nm. The photocatalytic properties of the catalysts for MO removal under different wavelengths were also estimated, and the results are depicted as in Fig. 5(e)–(h). Removal efficiencies and rate constants of MO by TiO_2 photocatalytic oxidation process under irradiation with different wavelengths are listed in Table 2. Result on dark degradation test showed only 1%–2% MO was adsorbed by the catalysts

Table 1
Some catalytic properties of undoped, Fe-doped and Zn-doped TiO_2

Doping amount (%)		Particle diameter [nm]			BET surface area [m^2/g]			Energy band gap [eV]		
		450°C	500°C	550°C	450°C	500°C	550°C	450°C	500°C	550°C
Undoped		14.4	16.0	31.8	68	60	23	3.06	3.02	2.98
Fe-	0.0005	14.1	15.9	30.5	72	64	23	3.04	3.00	2.95
	0.0010	13.9	15.6	20.0	73	67	57	3.00	2.95	2.89
	0.0050	13.7	15.2	26.3	78	78	32	2.96	2.88	2.83
Zn-	0.0005	12.4	13.8	22.4	97	96	52	3.05	3.00	2.97
	0.0010	13.2	14.7	17.0	95	93	76	3.05	2.99	2.95
	0.0050	12.2	13.3	19.0	101	97	69	3.01	2.95	2.91

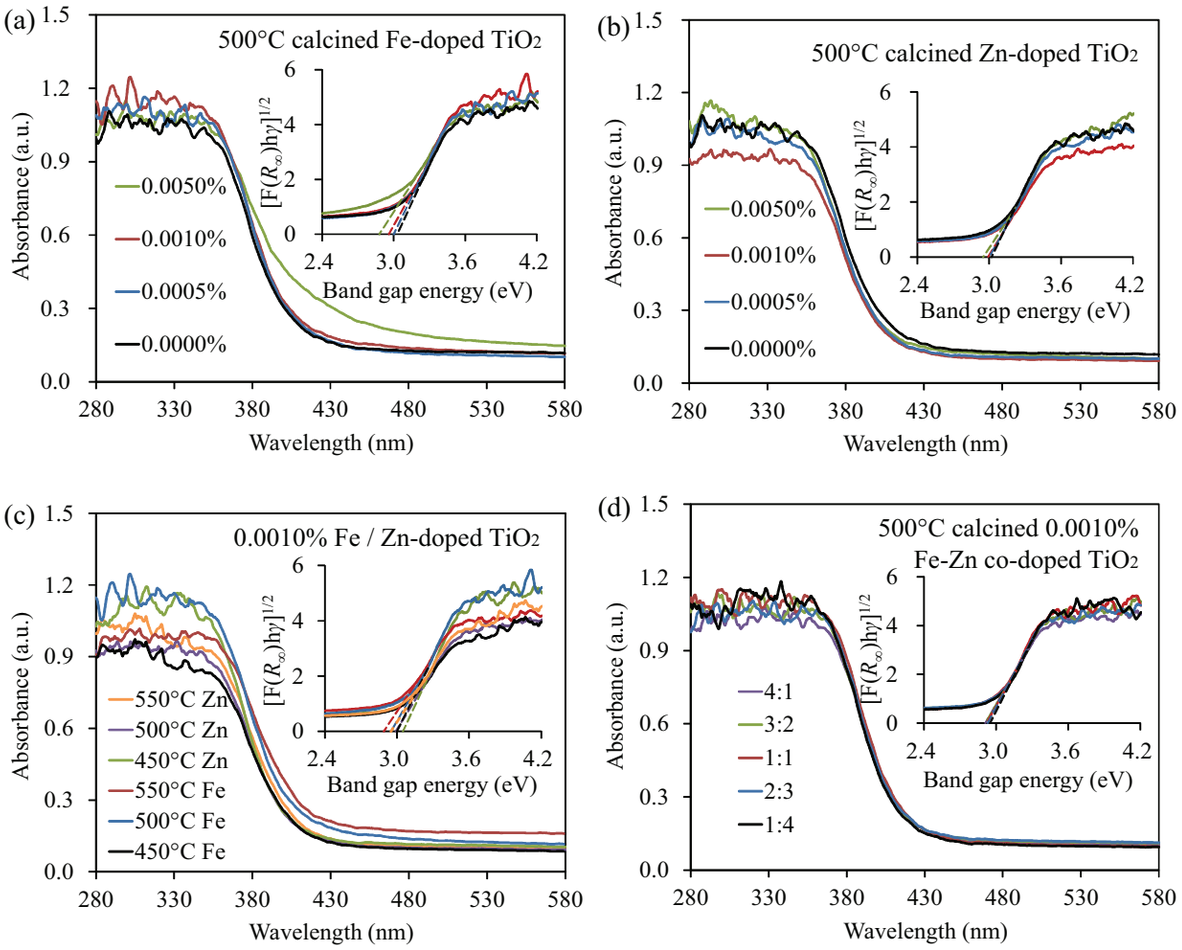

Fig. 4. DRS patterns and E_g of TiO_2.

when 0.5 g/L of catalysts were added, indicating that MO was mostly decomposed by oxidation.

(1) Effects of the calcination temperature

For undoped TiO_2, the highest catalytic activity was observed at calcination temperature of 450°C, with MO removal efficiency of 60.2% and pseudo-first-order rate constant of 0.189/h. The S_{BET}, crystalline phases and E_g of TiO_2 were crucial factors influencing the photocatalytic activity of the catalysts [2]. When the calcination temperature increased, the S_{BET} decreased (see Table 1), the E_g of TiO_2 was narrowed, and better crystallites were formed. For TiO_2 calcined at 500 and 550°C, although it had better crystalline phases and narrower E_g, the S_{BET} was smaller, and the overall efficiencies were low. TiO_2 calcined at 450°C had favorite crystallinity, S_{BET} and E_g, making it showed higher photocatalytic activity.

For Fe- or Zn-doped TiO_2, the photocatalytic activities of the catalysts were also affected by calcination temperature, and the reasons were more or less the same as those for the undoped ones. The optimal calcination temperatures for Fe-doped TiO_2 with the doping amount of 0.0005%, 0.0010% and 0.0050% were 450, 500 and 450°C, corresponding to the MO removal efficiencies of 60.0%, 48.9% and 54.8%, respectively. The best calcination temperatures for Zn-doped TiO_2 were same as those for Fe-doped TiO_2, and the MO removal efficiencies were 62.1%, 66.5% and 56.3%, respectively.

(2) Effects of the dopants

It can be seen from Fig. 5 and Table 2 that the MO decomposition rate increased when the catalysts were doped with Fe^{3+} or Zn^{2+}.

Fe^{3+} or Zn^2 doping can increase the photocatalytic activity of TiO_2 since the doping ions in the catalyst can affect the space charge region potential of the catalysts [24], and therefore change the property of TiO_2. The ions-doped TiO_2 had better crystalline phase, larger S_{BET} and narrower E_g than the undoped one. Therefore, MO removal efficiency in the presence of the Fe-doped or Zn-doped TiO_2 was higher. In addition, the dopant amount could also impact the photocatalytic activities of TiO_2. For both Fe-doped and Zn-doped TiO_2, highest

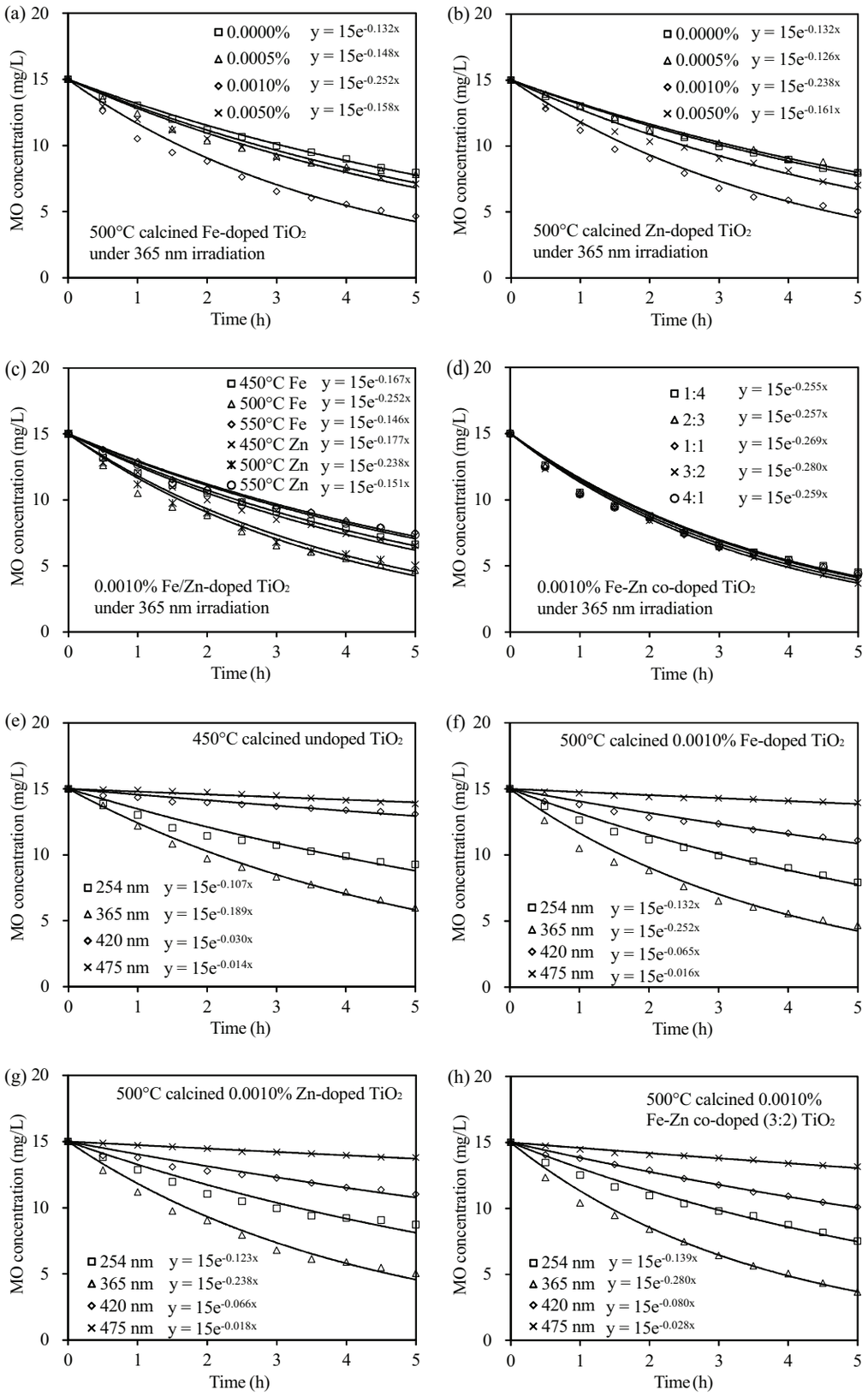

Fig. 5. Photocatalytic oxidation of 15 mg/L MO in the presence of TiO_2 under irradiation with different wavelengths.

Table 2
Removal efficiencies and rate constants of MO by TiO_2 photocatalytic oxidation process under irradiation with different wavelengths

TiO_2 catalysts			Removal efficiency [%]				Rate constant [/h]				Quantum yields [/(h·cd)]			
			254 nm	365 nm	420 nm	475 nm	254 nm	365 nm	420 nm	475 nm	254 nm	365 nm	420 nm	475 nm
Undoped	450°C		38.2	60.2	12.7	7.6	0.107	0.189	0.030	0.014	0.139	0.300	0.067	0.047
	500°C		30.5	46.9	11.8	6.3	0.076	0.132	0.028	0.013	0.099	0.210	0.062	0.043
	550°C		28.1	45.2	11.4	4.5	0.072	0.129	0.024	0.010	0.094	0.205	0.053	0.033
Fe-doped	450°C	0.0005%	40.9	60.0	19.3	8.9	0.112	0.190	0.048	0.016	0.145	0.302	0.107	0.053
		0.0010%	37.1	55.9	23.1	8.9	0.088	0.167	0.054	0.016	0.114	0.265	0.120	0.053
		0.0050%	34.6	54.8	26.5	10.0	0.086	0.166	0.065	0.020	0.112	0.263	0.144	0.067
	500°C	0.0005%	30.6	47.9	18.9	6.4	0.078	0.148	0.045	0.014	0.101	0.235	0.100	0.047
		0.0010%	47.3	68.9	25.9	6.9	0.132	0.252	0.065	0.016	0.171	0.400	0.144	0.053
		0.0050%	33.1	52.7	27.8	10.0	0.083	0.158	0.068	0.022	0.108	0.251	0.151	0.073
	550°C	0.0005%	29.2	46.3	18.8	4.9	0.073	0.124	0.040	0.010	0.095	0.197	0.089	0.033
		0.0010%	31.5	49.8	24.5	6.0	0.080	0.146	0.060	0.011	0.104	0.232	0.133	0.037
		0.0050%	32.5	52.2	23.3	5.2	0.081	0.157	0.053	0.010	0.105	0.249	0.118	0.033
Zn-doped	450°C	0.0005%	41.5	62.1	20.2	9.5	0.112	0.196	0.048	0.020	0.145	0.311	0.107	0.067
		0.0010%	38.8	56.5	24.4	9.7	0.101	0.177	0.058	0.021	0.131	0.281	0.129	0.070
		0.0050%	34.9	56.3	27.4	10.5	0.087	0.176	0.068	0.022	0.113	0.279	0.151	0.073
	500°C	0.0005%	30.5	46.0	19.3	6.8	0.075	0.126	0.047	0.013	0.097	0.200	0.104	0.043
		0.0010%	41.9	66.5	26.5	8.1	0.123	0.238	0.066	0.018	0.160	0.378	0.147	0.060
		0.0050%	33.3	53.1	29.2	9.7	0.083	0.161	0.074	0.021	0.108	0.256	0.164	0.070
	550°C	0.0005%	29.2	45.6	19.0	4.9	0.077	0.120	0.044	0.011	0.100	0.190	0.098	0.037
		0.0010%	30.5	51.0	26.0	6.4	0.077	0.151	0.063	0.012	0.100	0.240	0.140	0.040
		0.0050%	31.1	52.1	22.4	5.8	0.078	0.156	0.045	0.012	0.101	0.248	0.100	0.040
Co-doped	500°C	1:4	47.3	69.9	29.6	10.8	0.132	0.255	0.075	0.022	0.171	0.405	0.167	0.073
		2:3	47.8	70.1	30.5	11.3	0.133	0.257	0.078	0.023	0.173	0.408	0.173	0.077
		1:1	48.8	72.3	31.9	11.7	0.136	0.269	0.079	0.025	0.177	0.427	0.176	0.083
		3:2	49.9	75.5	32.7	12.3	0.139	0.280	0.080	0.028	0.181	0.444	0.178	0.093
		4:1	48.5	70.6	31.1	11.2	0.135	0.259	0.080	0.024	0.175	0.411	0.178	0.080

catalytic activities were observed at the calcination temperature of 500°C and doping amount of 0.0010%, with MO removal efficiency (rate constant) of 68.9% (0.252 /h) and 66.5% (0.238 /h), respectively.

The MO removal efficiencies in the presence of the Fe-Zn co-doped TiO_2 were higher than those in the presence of mono-doped TiO_2, which could be attributed to the synergetic co-doping effects of Fe and Zn into TiO_2. The S_{BET} increased when two metal ions were used as dopants. In addition, the *Eg* of co-doped TiO_2 was not considerably wider than that of the Fe-doped one. The 500°C calcined 0.0010% Fe-Zn co-doped TiO_2 with the Fe:Zn radio of 3:2 showed the highest catalytic activity, with the MO removal efficiency of 75.5% and rate constant of 0.280 /h, respectively.

(3) Effects of the irradiation wavelength

In all cases of our experiments, the order of the effectiveness of xenon lamp was 365 nm > 254 nm > 420 nm > 475 nm. When the electric current was 15 A, the light intensities at 254, 365, 420 and 475 nm were measured to be 0.77, 0.63, 0.45 and 0.30 cd, respectively. Generally, higher light intensity leaded to higher MO removal efficiency. Nevertheless, better decomposition effect was achieved at 365 nm because of the better penetrability of light at 365 nm than at 254 nm. In order to avoid the influence of the light intensity, the quantum yields were calculated (see Table 2), and the similar order of the effectiveness wavelength was obtained except for the TiO_2 with Fe or Zn dopant amount of 0.0050%. That was because for these catalysts, the E_g were in the range of 2.83 to 2.96 eV, corresponding to the wavelength of 438 to 419 nm, which was included when light source of 420 nm was used.

The E_g of the synthesized TiO_2 were in the range of 2.91 to 3.06 eV, meaning that TiO_2 can only be excited under irradiation of UV light at wavelengths less than 426 nm. However, MO could be degraded under the condition of light irradiation and air aeration. MO was decomposed mainly by photolysis under 475 nm irradiation, and the natural light in the laboratory could promote the photocatalytic degradation of MO since the reactor was not protected from light during the experiments. The MO removal efficiency was related to the S_{BET} of the catalysts. The 500°C calcined 0.0010% Fe-Zn co-doped TiO_2 with Fe:Zn radio of 3:2 showed the highest catalytic activity (12.3%) because of its largest S_{BET}.

When the wavelength of the light source reduced to be 420 ± 15 nm (corresponding to the E_g of 2.95 ± 0.10 eV), MO removal efficiencies in the presence of the catalysts increased. In most cases, the photocatalytic activity of the catalyst increased with the increase of the calcination temperature and the doping amount of the dopants as TiO_2 with wider E_g could be excited under irradiation with the wavelength of 420 nm.

The decomposition effect of MO using the synthesized photocatalysts under 254 nm and 365 nm of UV light irradiation was related to the S_{BET}, crystalline phases and E_g of the catalysts. Highest MO removal efficiency was obtained in the presence of the 500°C calcined 0.0010% Fe-Zn co-doped TiO_2 (Fe:Zn = 3:2), with the MO removal efficiencies of 49.9% and 75.5% for the experiment under irradiation of 254 nm and 365 nm, respectively.

3.2.2. Mechanism of MO degradation

The chromatograms of MO after 5 h UV irradiation and photocatalytic oxidation at pH 7 are presented in Fig. 6. The chromatograms show the appearance of peaks corresponding to the by-products from the degradation of MO. It is evident that similar by-products were formed during both UV irradiation and photocatalytic oxidation. Nearly 60% of MO was removed by UV irradiation in 5 h, and many intermediate species (Products A–D) were still present in the solution after 5 h. However, MO was completely decomposed via photocatalytic oxidation during 3 h.

The molecular structures of the by-products were deduced by analyzing the samples with MS/MS and comparing the results from the literatures [25–29], and the proposed degradation pathway is shown in Fig. 7. MO (retention time 7.81 min), exhibited a clear MS signal corresponding to a negative ion m/z 304.

For UV irradiation process, the degradation of MO was initiated by the attack of ·OH radicals resulting in aromatic substitution of one of the benzene rings of MO with hydroxyl group, leading to the formation of Product B (retention time 5.43 min, m/z 320) [30]; Product D (retention time 7.22 min, m/z 290) was a demethylated intermediate formed by the rupture of the -N-C- bond of the amine group which led to the substitution of one methyl group with a hydrogen atom [31]; Product C (retention time 6.26 min, m/z 276) was formed by the cleavage of another methylene group from the amine group [26,30]. Further, the -N-C- band which linked to the benzene ring with high bond energy was disconnected [30], resulting in the formation of Product A (retention time 4.79 min, m/z 141) and other low molecular weight degradation products. After irradiation for 3 h, the peak intensities of MO and its products did not change significantly, and the peak of Product A was extremely low. It could be obtained from the result that MO could not be oxidized completely by UV irradiation, and several by-products were emerged during this process.

For the photocatalytic oxidation process, MO was degraded by similar pathway, and Products C and D were formed. Further, the benzene ring, as well as the branched-chains linking to the benzene ring, was broken, and the -N=N- band, which named as azo bond, was also cleaved. After that, the organic structures were mineralized during the complete oxidation process without the formation of Product A, showing non-selectivity and better oxidizability of the photocatalysis process.

3.3. Photocatalytic activity of GAC supported TiO_2

3.3.1. Effect of GAC supporting

The removal of MO in the presence of GAC supported Fe-Zn co-doped TiO_2 is shown in Fig. 8. The elimination of MO in photocatalytic oxidation process in the presence of GAC supported co-doped TiO_2 was 75.5%, higher than in the presence of the dispersive co-doped TiO_2. This indicated that the adsorption capacity of GAC supported co-doped TiO_2 was substantially higher than naked TiO_2 as expected [32]. However, the photocatalytic degradation efficiency only slightly increased. Higher adsorption efficiency meant

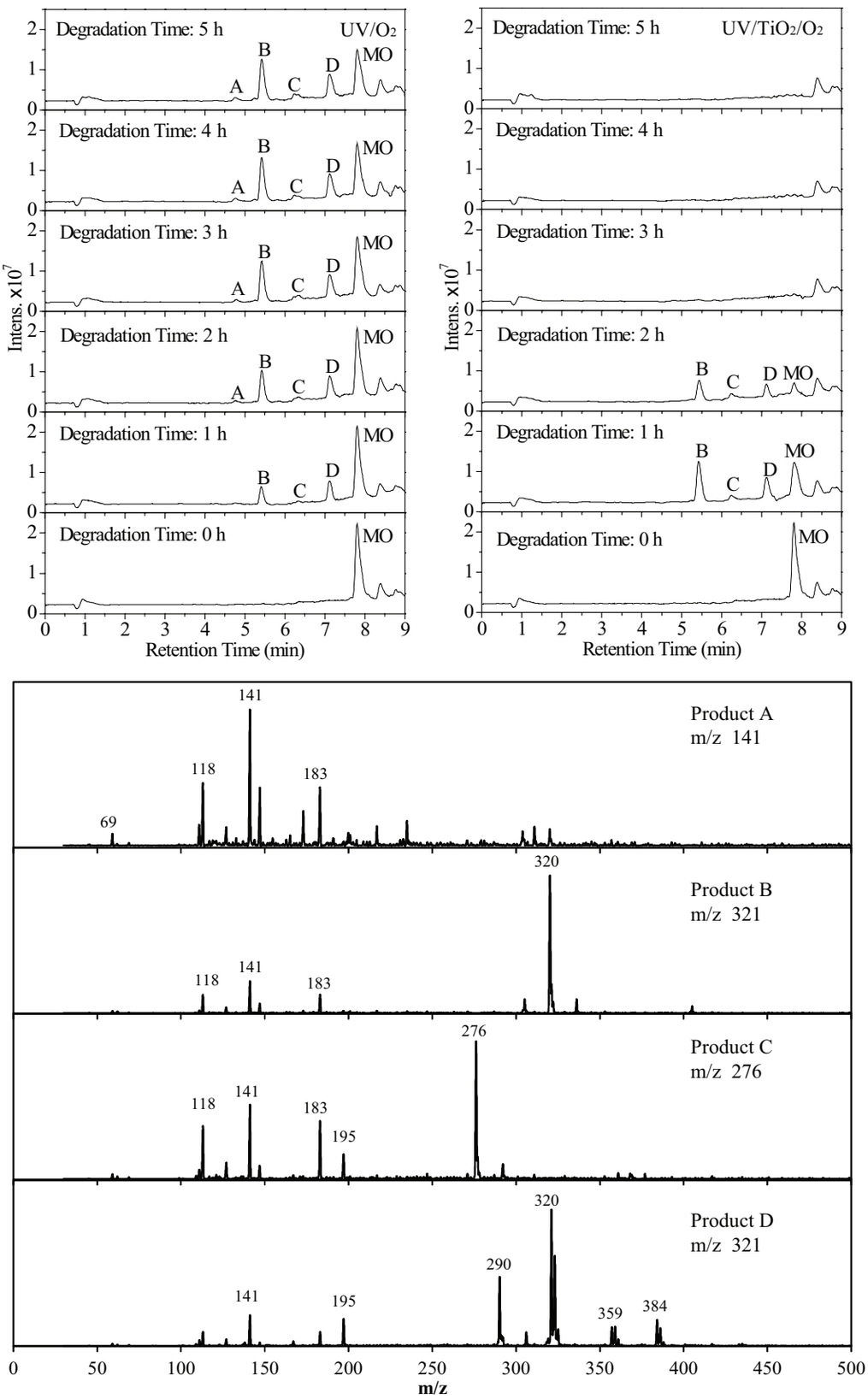

Fig. 6. Chromatographs observed during UV irradiation and photocatalytic degradation of 15 mg/L MO.

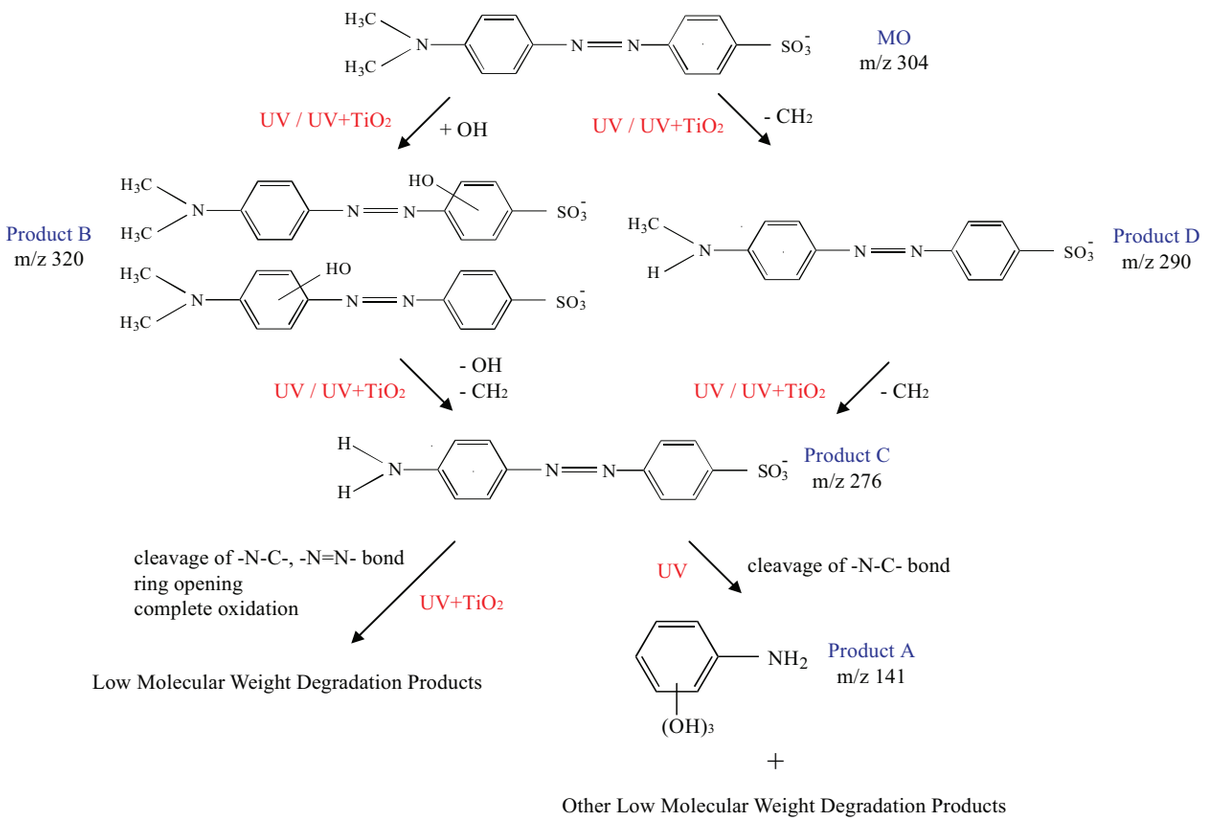

Fig. 7. Proposed pathway for MO degradation under UV irradiation or photocatalytic degradation in the presence of Fe-Zn co-doped TiO_2.

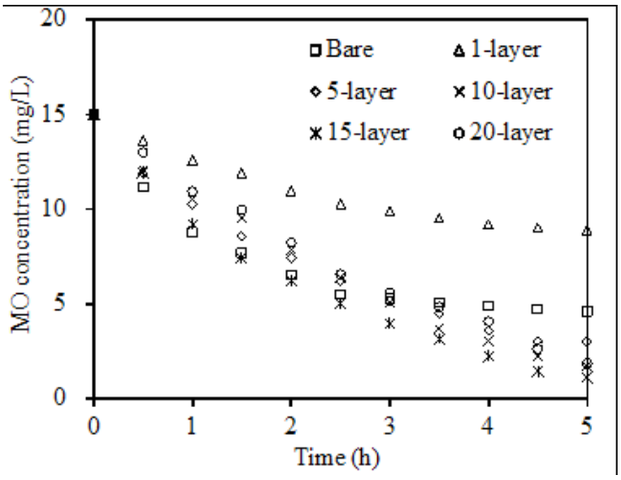

Fig. 8. Photocatalytic degradation of 15 mg/L MO in the presence of GAC supported TiO_2.

the degradation efficiency was increased to a lesser extent because an excessive number of MO molecules adsorbed onto the surface of the photocatalysts hindered photons from reaching the surface of the photocatalysts [33].

The coating amount of co-doped TiO_2 can affect the removal efficiency of MO [34]. GAC coated with 15-layer of TiO_2 was proved to be the best composition with respect to catalytic activity, corresponding to the MO removal efficiency of 92.5%. The catalytic activities for the catalysts were in the order of 15-layer > 10-layer > 20-layer > 5-layer > bare GAC > 1-layer. In most cases, the removal efficiency of MO in the presence of GAC coated with co-doped TiO_2 was higher than that in the presence of GAC adsorption due to the photocatalytic activity of the TiO_2 on the surface of GAC. The MO elimination was affected by the TiO_2 amount because when GAC was coated with TiO_2, the S_{BET} changed. The S_{BET} for GAC supported catalysts with the coating amount of 1, 5, 10, 15 and 20 layers were 669, 632, 614, 591 and 567 m^2/g, respectively, while the S_{BET} of bare GAC was 785 m^2/g. The S_{BET} decreased with the increase of the coating amount, resulting in the reduction of the adsorption capacity. However, the MO removal efficiency by 1-layer-TiO_2 coated GAC was lower than by bare GAC because some of the pore in GAC was overlapped with TiO_2, while the amount of TiO_2 was too low to promote the decomposition of MO. For the 20-layer-TiO_2 coated GAC, although the amount of the co-doped TiO_2 catalyst was large, the adsorption capacity of GAC was extremely low, resulting in the lower MO removal efficiency than 15-layer-TiO_2 coated GAC.

During the first 2.5 h of irradiation, high degradation rates of MO were observed due to the free surface of activated carbon at early stage which led to higher adsorbability of the catalyst [32]. Then, the residence time and

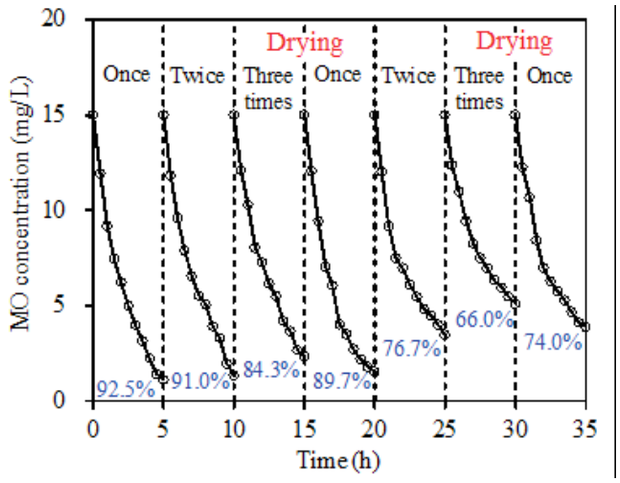

Fig. 9. Reusability of the GAC supported TiO_2 catalysts.

concentration of the MO molecules close to TiO_2 catalyst was artificially increased because of the concentrated effect [35,36]. The active oxidizing chemical species diffused from the co-doped TiO_2, where they were formed, to the adsorbent sites on which the pollutants were adsorbed [36], and then reacted with MO. The on-stream continuous regeneration of the adsorption sites of GAC occurred due to the intimate contact between both adsorption and photocatalytic sites. In addition, the intimate contact between GAC and TiO_2 could allow the transfer of the excited electrons from the TiO_2 conduction band to the surface of GAC to be effective, and thus decreased the TiO_2 charge recombination [37].

3.3.2. Reusability of the GAC supported TiO_2

The recycle experiment on the photocatalytic decoloration of MO solution was carried out, and the results are displayed in Fig. 9. The removal efficiencies of MO reached 92.5%, 91.0% and 84.3% after the 3 degradation cycles, respectively. It can be observed that the decoloration ratio was just slightly degressive with the increase in cycle times, indicating that cyclic usage of the photocatalyst was possible. It also proves that the final removal of MO from solutions was caused by the photocatalytic degradation other than the adsorption process that would lead to saturated adsorption of MO on the photocatalyst [38]. The decrease of the degradation activity during the recycling processes could be attributed to the residual MO and intermediates being strongly adsorbed onto and inside the photocatalyst [39].

The MO removal efficiency increased from 84.3% to 89.7% by drying the catalyst before use, indicating that some of the residuals could desorb from GAC by drying. Therefore, the photocatalytic activity of the catalysts can be partly improved by drying them.

4. Conclusions

MO was effectively degraded in the presence of Fe-doped, Zn-doped or Fe-Zn co-doped TiO_2 under irradiation with 365 nm UV light. The photocatalytic activities of the catalysts were affected by the calcination temperature and the doping amount of the dopants, which could impact the S_{BET}, E_g and crystallinity of the catalysts. The optimal calcination temperature was 500°C for both Fe-doped and Zn-doped TiO_2, and the best photocatalytic activities were achieved when the Fe^{3+} or Zn^{2+} doping amount was 0.0010%. Highest MO removal efficiency was achieved in the presence of 500°C calcined 0.0010% Fe-Zn co-doped TiO_2 with the Fe:Zn radio of 3:2.

For MO photocatalytic oxidation, the order of the effectiveness of xenon lamp was 365 nm > 254 nm > 420 nm > 475 nm. Generally, higher light intensity leaded to higher MO removal efficiency. However, the degradation of the pollutants was faster under 365 nm irradiation because of the better penetrability of light at 365 nm than at 254 nm. The structures of the intermediates formed during UV irradiation process were based mainly on demethylation and cleavage of -N-C- bond. For the photocatalytic oxidation process, MO was degraded followed the similar pathway, except that almost all the pollutants was decomposed to be the inorganic substance.

The elimination of MO in photocatalytic oxidation process by GAC supported Fe-Zn co-doped TiO_2 was higher than dispersive TiO_2. GAC coated with 15-layer of co-doped TiO_2 was proved to be the best composition with respect to catalytic activity, and the catalytic activities for the catalysts were in the order of 15-layer > 10-layer > 20-layer > 5-layer > 1-layer. The decoloration ratio was just slightly degressive with the increase in cycle times, indicating that cyclic usage of the photocatalyst is possible. The photocatalytic activity of the catalysts could be improved by drying.

Acknowledgment

We gratefully acknowledge the National Science and Technology Major Projects Special for Water Pollution Control and Management (No. 2015ZX07203-011), the State Scholarship Fund of China Scholarship Council (No. 201706465019), and the financial support from the Fundamental Research Funds for the Central Universities of China (FRF-TP-15-047A1).

References

[1] Z. Zhang, Y. Xu, X. Ma, F. Li, D. Liu, Z. Chen, F. Zhang, D.D. Dionysiou, Microwave degradation of methyl orange dye in aqueous solution in the presence of nano-TiO_2-supported activated carbon (supported-TiO_2/AC/MW), J. Hazard. Mater., 209–210 (2012) 271–277.
[2] Y.L. Pang, A.Z. Abdullah, Effect of low Fe^{3+} doping on characteristics, sonocatalytic activity and reusability of TiO_2 nanotubes catalysts for removal of Rhodamine B from water, J. Hazard. Mater., 235–236 (2012) 326–335.
[3] R. Yuan, B. Zhou, D. Hua, C. Shi, Enhanced photocatalytic degradation of humic acids using Al and Fe co-doped TiO_2 nanotubes under UV/ozonation for drinking water purification, J. Hazard. Mater., 262 (2013) 527–538.
[4] S. Peng, Y. Li, F. Jiang, G. Lu, S. Li, Effect of Be^{2+} doping TiO_2 on its photocatalytic activity, Chem. Phys. Lett., 398(1) (2004) 235–239.
[5] Y. Li, S. Peng, F. Jiang, G. Lu, S. Li, Effect of doping TiO_2 with alkaline-earth metal ions on its photocatalytic activity, J. Serb. Chem. Soc., 72(4) (2007) 393–402.

[6] Y. Li, Y. Xiang, S. Peng, X. Wang, L. Zhou, Modification of Zr-doped titania nanotube arrays by urea pyrolysis for enhanced visible-light photoelectrochemical H_2 generation, Electrochim. Acta, 87 (2013) 794–800.
[7] Y. Li, Y. Jiang, S. Peng, F. Jiang, Nitrogen-doped TiO_2 modified with NH_4F for efficient photocatalytic degradation of formaldehyde under blue light-emitting diodes, J. Hazard. Mater., 182 (2010) 90–96.
[8] D. Hou, R. Goei, X. Wang, P. Wang, T.-T. Lim, Preparation of carbon-sensitized and Fe–Er codoped TiO_2 with response surface methodology for bisphenol A photocatalytic degradation under visible-light irradiation, Appl. Catal. B Environ., Appl. Catal. B Environ., 126 (2012) 121–133.
[9] Y. Li, G. Ma, S. Peng, G. Lu, S. Li, Boron and nitrogen co-doped titania with enhanced visible-light photocatalytic activity for hydrogen evolution, Appl. Surf. Sci., 254(21) (2008) 6831–6836.
[10] S. Naraginti, T.V. Thejaswini, D. Prabhakaran, A. Sivakumar, V.S. Satyanarayana, A.S. Arun Prasad, Enhanced photo-catalytic activity of Sr and Ag co-doped TiO_2 nanoparticles for the degradation of Direct Green-6 and Reactive Blue-160 under UV & visible light, Spectrochim. Acta A, 149 (2015) 571–579.
[11] H. Eskandarloo, A. Badiei, M.A. Behnajady, G.M. Ziarani, Ultrasonic-assisted sol-gel synthesis of samarium, cerium co-doped TiO_2 nanoparticles with enhanced sonocatalytic efficiency, Ultrason. Sonochem., 26 (2015) 281–292.
[12] M. Sanchez-Dominguez, G. Morales-Mendoza, M.J. Rodriguez-Vargas, C.C. Ibarra-Malo, A.A. Rodriguez-Rodriguez, A.V. Vela-Gonzalez, S.A. Perez-Garcia, R. Gomez, Synthesis of Zn-doped TiO_2 nanoparticles by the novel oil-in-water (O/W) microemulsion method and their use for the photocatalytic degradation of phenol, J. Environ. Chem. Eng., 3 (2015) 3037–3047.
[13] R. Yuan, B. Zhou, D. Hua, C. Shi, L. Ma, Effect of metal-ion doping on the characteristics and photocatalytic activity of TiO_2 nanotubes for the removal of toluene from water, Water Sci. Technol., 69 (2014) 1697–1704.
[14] M.R. Eskandarian, H. Choi, M. Fazli, M.H. Rasoulifard, Effect of UV-LED wavelengths on direct photolytic and TiO_2 photocatalytic degradation of emerging contaminants in water, Chem. Eng. J., 300 (2016) 414–422.
[15] H. Chaker, L. Chérif-Aouali, S. Khaoulani, A. Bengueddach, S. Fourmentin, Photocatalytic degradation of methyl orange and real wastewater by silver doped mesoporous TiO_2 catalysts, J. Photoch. Photobio. A, 318 (2016) 142–149.
[16] V.K. Gupta, R. Saravanan, S. Agarwal, F. Gracia, M.M. Khan, J. Qin, R.V. Mangalaraja, Degradation of azo dyes under different wavelengths of UV light with chitosan-SnO_2 nanocomposites, J. Mol. Liq., 232 (2017) 423–430.
[17] R. Yuan, B. Zhou, L. Ma, Removal of toluene from water by photocatalytic oxidation with activated carbon supported Fe^{3+}-doped TiO_2 nanotubes, Water Sci. Technol., 70 (2014) 642–648.
[18] H.D. Mansilla, A. Mora, C. Pincheira, M.A. Mondaca, P.D. Marcato, N. Durán, J. Freer, New photocatalytic reactor with TiO_2 coating on sintered glass cylinders, Appl. Catal. B Environ., 76 (2007) 57–63.
[19] Y. Huo, Z. Xie, X. Wang, H. Li, M. Hoang, R.A. Caruso, Methyl orange removal by combined visible-light photocatalysis and membrane distillation, Dyes Pigments, 98 (2013) 106–112.
[20] L. Ravichandran, K. Selvam, B. Krishnakumar, M. Swaminathan, Photovalorisation of pentafluorobenzoic acid with platinum doped TiO_2, J. Hazard. Mater., 167 (2009) 763–769.
[21] L. Deng, S. Wang, D. Liu, B. Zhu, W. Huang, S. Wu, S. Zhang, Synthesis, characterization of Fe-doped TiO_2 nanotubes with high photocatalytic activity, Catal. Lett., 129 (2009) 513–518.
[22] J. Xiao, Y. Xie, H. Cao, F. Nawaz, S. Zhang, Y. Wang, Disparate roles of doped metal ions in promoting surface oxidation of TiO_2 photocatalysis, J. Photoch. Photobio. A, 315 (2016) 59–66.
[23] S. Sood, A. Umar, S.K. Mehta, S.K. Kansal, Highly effective Fe-doped TiO_2 nanoparticles photocatalysts for visible-light driven photocatalytic degradation of toxic organic compounds, J. Colloid Interf. Sci., 450 (2015) 213–223.
[24] H.E. Chao, Y.U. Yun, H.U. Xingfang, A. Larbot, Effect of silver doping on the phase transformation and grain growth of sol-gel titania powder, J. Eur. Ceram. Soc., 23 (2003) 1457–1464.
[25] A. Mondal, B. Adhikary, D. Mukherjee, Room-temperature synthesis of air stable cobalt nanoparticles and their use as catalyst for methyl orange dye degradation, Colloids Surf. A Physicochem. Eng. Asp., 482 (2015) 248–257.
[26] Y. He, F. Grieser, M. Ashokkumar, The mechanism of sonophotocatalytic degradation of methyl orange and its products in aqueous solutions, Ultrason. Sonochem., 18 (2011) 974–980.
[27] T. Chen, Y. Zheng, J.M. Lin, G. Chen, Study on the photocatalytic degradation of methyl orange in water using Ag/ZnO as catalyst by liquid chromatography electrospray ionization ion-trap mass spectrometry, J. Am. Soc. Mass Spectr., 19 (2008) 997–1003.
[28] H. Li, J. Guo, L. Yang, Y. Lan, Degradation of methyl orange by sodium persulfate activated with zero-valent zinc, Sep. Purif. Technol., 132 (2014) 168–173.
[29] S. Filice, D. D'Angelo, S. Libertino, I. Nicotera, V. Kosma, V. Privitera, S. Scalese, Graphene oxide and titania hybrid Nafion membranes for efficient removal of methyl orange dye from water, Carbon, 82 (2015) 489–499.
[30] J. Kaur, S. Singhal, Facile synthesis of ZnO and transition metal doped ZnO nanoparticles for the photocatalytic degradation of Methyl Orange, Ceram. Int., 40 (2014) 7417–7424.
[31] F. Huang, L. Chen, H. Wang, T. Feng, Z. Yan, Degradation of methyl orange by atmospheric DBD plasma: analysis of the degradation effects and degradation path, J. Electrost., 70 (2012) 43–47.
[32] M. Gar Alalm, A. Tawfik, S. Ookawara, Enhancement of photocatalytic activity of TiO_2 by immobilization on activated carbon for degradation of pharmaceuticals, J. Environ. Chem. Eng., 4 (2016) 1929–1937.
[33] F.T. Li, Y. Zhao, Y.J. Hao, X.J. Wang, R.H. Liu, D.S. Zhao, D.M. Chen, N-doped P25 TiO_2-amorphous Al_2O_3 composites: one-step solution combustion preparation and enhanced visible-light photocatalytic activity, J. Hazard. Mater., 239–240 (2012) 118–127.
[34] J.W. Shi, H.J. Cui, J.W. Chen, M.L. Fu, B. Xu, H.Y. Luo, Z.L. Ye, TiO_2/activated carbon fibers photocatalyst: effects of coating procedures on the microstructure, adhesion property, and photocatalytic ability, J. colloid Interf. Sci., 388 (2012) 201–208.
[35] Y. Li, J. Wang, S. Peng, G. Lu, S. Li, Photocatalytic hydrogen generation in the presence of glucose over ZnS-coated $ZnIn_2S_4$ under visible light irradiation, Int. J. Hydrogen. Energy, 35(13) (2010) 7116–7126.
[36] M. Lafjah, F. Djafri, A. Bengueddach, N. Keller, V. Keller, Beta zeolite supported sol-gel TiO_2 materials for gas phase photocatalytic applications, J. Hazard. Mater., 186 (2011) 1218–1225.
[37] A.C. Martins, A.L. Cazetta, O. Pezoti, J.R.B. Souza, T. Zhang, E.J. Pilau, T. Asefa, V.C. Almeida, Sol-gel synthesis of new TiO_2/activated carbon photocatalyst and its application for degradation of tetracycline, Ceram. Int., 43 (2017) 4411–4418.
[38] P. Fu, Y. Luan, X. Dai, Preparation of activated carbon fibers supported TiO_2 photocatalyst and evaluation of its photocatalytic reactivity, J. Mol. Catal. A, 221 (2004) 81–88.
[39] R. Ma, X. Wang, J. Huang, J. Song, J. Zhang, X. Wang, Photocatalytic degradation of salicylic acid with magnetic activated carbon-supported F-N codoped TiO_2 under visible light, Vacuum, 141 (2017) 157–165.